Graphical Abstract:

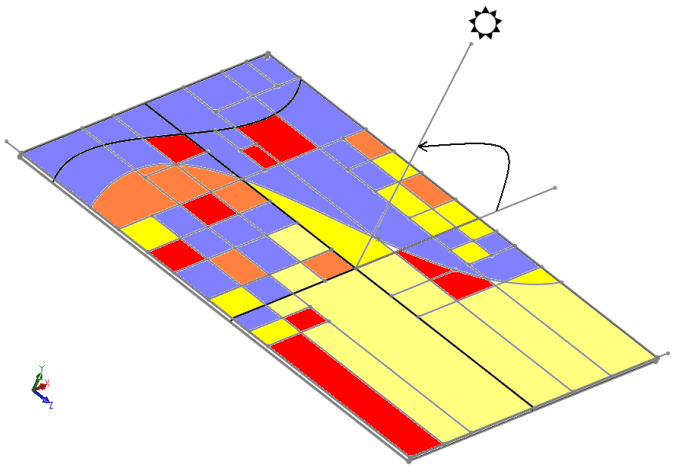

Highlights:

- Performance of 70 different luminescent solar concentrators (LSC) were evaluated
- LSC sheets: 5 different fluorescent organic dyes each at 7 different concentrations
- Ray-tracing results within in good agreement (±13%) of experimental measurements
- Greater confidence now in use LSCs for building integrated photovoltaics
- Stained-glass window LSC developed and performance modelled

Luminescent Solar Concentrators: from Experimental Validation of 3D Ray-Tracing Simulations to Coloured Stained-Glass Windows for BIPV

A. Kerrouche[1], D.A. Hardy[1], D. Ross[1], B. S. Richards[1,2*]

[1] School of Engineering and Physical Sciences, Heriot-Watt University, Edinburgh, EH14 4AS, United Kingdom

[2] Department of Materials Science & Engineering Nelson Mandela African Institute of Science and Technology, Tengeru, Arusha, Tanzania

Abstract

Luminescent solar concentrators (LSC) are a promising technology for building integrated photovoltaics (BIPV) given the wide variety of forms and colours that can be realised. Given the flexibility of the technology, the use of ray-trace modelling is indispensable in the design, performance evaluation, and optimisation of LSCs. This work begins by comparing a three-dimensional (3D) ray-trace model of an LSC with experimental results. The study includes 70 samples – both square and circular LSCs, containing five different fluorescent organic dyes (BASF Lumogen) each at seven different concentrations. The figure-of-merit used for performance evaluation was the average power density determined at the LSC edge sheet, measured using an optical fibre connected to a spectrometer. The results demonstrate that 3D ray-trace results gives good agreement with the experimental measurements, to within around ±5% within a wide concentration range (optical density = 0.05 – 8) and a maximum difference of ±13%. The wide range of colours achieved is presented in a CIE chart. Overall, the validated experimental results give confidence in the use of modelling for future larger LSCs for BIPV. Therefore, based on these results and the colours achievable, a model of a stained-glass window is constructed and its performance throughout a solar day is simulated.

Keywords: luminescent solar concentrator; fluorescent dye; photovoltaic; building integrated photovoltaics; ray-tracing; window

* Corresponding author: Bryce Richards, email: b.s.richards@hw.ac.uk

1. Introduction

Concentrating photovoltaic (CPV) systems have progressed considerably in the last few years, and are now establishing their potential as a cost effective solution by reducing the area of solar cells and using less expensive materials [1]. The majority of CPV technologies rely on a system of lenses or mirrors to concentrate the direct beam of the sun onto a high efficiency solar cell, and are thus well-suited for large installations in sunny regions of the Earth. On the other hand, the luminescent solar concentrator (LSC) is a low-concentrating technology that is able to effectively harvest both diffuse and direct sunlight. The first publications on LSCs were by Weber and Lambe in 1976 [2] and Goetzberger and Greubel in 1977 [3]. Since then, this technology has been extensively studied and developed with a particular focus on building-integrated photovoltaics (BIPV) for cloudier European climates [4-8].

The LSC consists of a transparent medium such as a polymer sheet, doped with a low concentration of fluorescent organic dyes. These dyes absorb a fraction of the incident sunlight and emit photons with a near unity quantum yield. The luminescence is trapped within the LSC sheet and transported to the edge via total internal reflection (TIR), as shown in Figure 1. TIR occurs only if the angle of luminescence emission from the dye is greater than a critical angle called the escape cone θ_C which can be calculated from the following equation:

$$\theta_C = \sin^{-1}\left(\frac{1}{n}\right), \tag{1}$$

where n is the refractive index of the host material, typically n~1.5 for polymer or glass waveguides. Luminescence reaching the edge of the LSC is converted into electricity by solar cells attached to the edges of the polymer sheet.

The use of modelling to predict the performance of PV devices coupled with luminescent materials has been investigated via different approaches. Firstly, thermodynamic analyses have been performed for planar LSCs, which show results in good agreement with experiments [9]. Secondly, ray-tracing or Monte-Carlo models for fluorescent concentrators proposed in the early 1980s by Heidler *et al.* [10] for an efficiency analysis, and Carrascosa *et al.* [11] for thin-film LSCs under both direct and diffuse light. Since then, many models have been developed for LSCs based on fluorescent organic dyes and semiconductor quantum dots [12–14]. Also, Meyer *et al.* [15] have used ray-tracing to compare the re-absorption probability (analytical) model developed by Weber and Lambe [2], while McIntosh *et al.* extended the ray-tracing beyond flat sheets to cylindrical LSCs [16].

Thermodynamic models are mainly used to simulate simple LSC shapes under direct sunlight. The agreement between simulated and experimental results is around 4%. However, this approach is not flexible enough to model different shapes under diffuse sunlight. Ray-tracing modelling is more flexible at simulating several geometries under direct and diffuse sunlight. Ray-tracing models have achieved around 15% agreement with experimental results [10]. This accuracy of such a model is often constrained by the input data which needs to be measured, so precise input data is

even more essential for more complex shapes, larger dimensions, when mirrors are included, and for the absorption and emission properties of the luminescent materials themselves. Several simulation tools have improved significantly in the past few years, due to high speed computers, enhanced three-dimensional (3D) graphical interface software, and increased material properties databases. Also, the fact that the actual imported data as opposed to extrapolated into the modelling process helps to run simulations more efficiently and easier than using simulation with extrapolation to generate the input data as Heidler *et al.* [10]. So, the efficacy of the simulation software is not only dependent on the accuracy and the high-speed of its calculation but on the demonstration of a realistic modelling of a LSC which covers all the appropriate parameters.

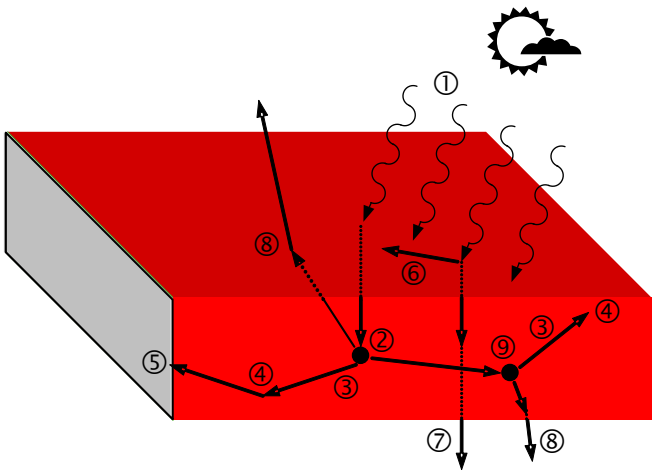

Figure 1. Cross-sectional diagram of a luminescent solar concentrator (LSC), showing how sunlight (①) is incident on the front surface, enters the LSC and encounters a fluorescent organic dye molecule (②) and is absorbed. The longer wavelength luminescence is re-emitted at a high photoluminescent quantum yield (PLQY, ③), and is then waveguided to the edge via total internal reflection (TIR, ④). Long, thin photovoltaic devices (⑤) are adhered to the edge of the LSC to convert the luminescence to DC electricity. The common loss mechanisms that are encountered include: ⑥ front surface reflection; ⑦ sunlight not being fully absorbed; ⑧ luminescence emitted within the critical angle being lost via front and rear escape cones; and, ⑨ luminescence being reabsorbed by another dye molecules due to overlapping absorption and emission spectra. Once the latter event occurs, this compounds previous losses via sub-unity PLQY (③) or escape cones (⑧). Note, that parasitic absorption within the host matrix is not depicted here, and neither is scattering of light from the LSC surfaces or within the bulk of the sheet.

In this study, the commercially available 3D ray-tracing simulation software Optisworks (Optis, France) is used to predict the transport of the trapped photons inside the LSC to the edge of the sheet, thus predicting the power output and optical efficiency. Most papers give detailed mathematical modelling without emphasis on which optimum concentrations and colours that could be used to create a new generation of building-integrated photovoltaics (BIPV). This aspect of our research, thus seeks to demonstrate how LSCs based on the different dye colours and concentrations will look like in BIPV and in artistic applications. This has important implications for the on-going debate between artists, architects and engineers on how to aesthetically integrate photovoltaics into architecture, considering trade-offs between: power; colour and light transmittance (or day lighting).

In this paper, a comparison between 3D ray-tracing simulation for LSC sheets and experimental results is carried out by the type of dye doped into the polymer sheet (and hence varying the colour of the LSC) and the concentration of each dye. A thorough comparison of experimental results from LSCs under simulated air-mass 1.5 global (AM1.5G) sunlight – fabricated in two different shapes, with five different dyes at seven different concentrations each – is conducted and excellent agreement with simulation results achieved. The performance parameters of the LSC are reported in terms of optical efficiency – defined as the output power density divided by the input power density – which is the most important parameter in determining the subsequent electrical performance. The optical efficiency along the edge of a square LSC and the influence of the tilt angle are also reported. Based on these results and the colours achievable, a model of a stained glass window (as shown in Figure 2) was constructed and its performance throughout a solar day simulated.

Figure 2: The stained glass window used for the modelling (47cm x 58cm x 0.3cm); this window was commissioned for a house in Bristol, U.K., and was designed by artist Carol Arnold [27].

2. Modelling

In general, ray-tracing techniques are used for optical analysis for the propagation of light. This propagation takes into account the optical properties of surfaces, materials and emission sources. The software launches rays into a model such as an LSC, and analyses each ray, which can be subjected to absorption, reflection, refraction, diffraction and scatter. As the rays propagate along different paths, surfaces and materials following the Snell-Descartes law, the software keeps track of the optical flux associated with each ray until it leaves the model. To achieve the effective modelling of an LSC, it is necessary to define the optical parameters of the florescent dyes and of the medium used for the simulation. The software requires the optical properties of the: i) host material – dispersive refractive index n and extinction coefficient k; as well as the ii) dye molecule properties – absorption spectrum, emission spectrum, and photoluminescence quantum yield (PLQY). The software considers the dye as a non-scattering material and the dye emission distribution is assumed to be isotropic. In addition to this, virtual detectors can be placed above the LSC, in order to calculate the escape cone losses, and along the edges measure the emitted energy flux. Having the potential to perform 3D ray-tracing is important for the study of LSC's, in order to

gain a complete understanding of the loss mechanisms and especially when more complicated designs with different colours and shapes are being considered for BIPV applications.

In this work, all ray-tracing simulations in this study were performed using Optisworks (Optis, France). The detectors were placed at a distance of 1 mm from the front surface for escape cone loss determination, and 1 mm from the side for determining the emitted power that could be harvested by edge-mounted solar cells. To match the experimental conditions as closely as possible, the diameter of the side detector was equal to the diameter of the cosine corrector. The optical constants *n* and *k* of the polymethylmethacrylate (PMMA) host, the dye absorption and emission spectra, as well as the PLQY values are all taken from Wilson and Richards [17]. The number of simulated rays was set to 100 million rays to reach a high level of precision in the results (>95%) while consuming very little memory about (150Mb for 1 million parameters). When running on a quad-core processor desktop computer, a typical simulation of 100 million rays took around 3 hours.

3. Experiment

In order to validate the simulation and to make a comparison between the mathematical modelling and the real model, a total of 70 LSC sheets were fabricated. The cast PMMA sheets were fabricated by Chilin (Taiwan) as part of a collaboration with Heriot-Watt University and BASF (Germany), who provided the Lumogen dyes. The thermally cast sheets had initial dimensions of about 45cm × 38cm. Out of these sheets, smaller LSC samples were cut and the edges diamond polished. Half of the LSC sheets were square with dimensions of 100mm × 100mm × 3mm, while the remainder were circular with a diameter of ∅100mm and thickness of 3 mm. The LSC sheets were doped with five different fluorescent organic dyes: BASF Lumogen F series Red 305, Yellow 170, Yellow 083, Orange240 and Violet 570. A wide range of concentrations were chosen to achieve an absorbance or optical density (OD) of 0.05, 1, 2, 3, 4, 8, and 16 with each dye. The OD = 0.05 samples were fabricated to avoid self-absorption as much as possible [18], while higher OD samples (OD = 1 – 4) are more typical of what would be used to fabricated a LSC. The highest concentrations (OD = 8, 16) were chosen to see how well the experiment would match the simulation under more extreme conditions. Overall, these dyes are chosen because of their near unity PLQY, availability in a wide range of colours, and good environmental stability [19-21]. Table 1 details the exact dye concentrations used to fabricated the 70 LSC sheets.

Measurements of LSC performance were conducted under a xenon-based solar simulator (ABET Technologies Sun2000 11044, class AAB, 1000W continuous) equipped with quartz optics and both AM1.5G and ultraviolet (UV) edge filters. The resulting spectrum is a better than class A match (within ±15%) to the AM1.5G spectrum down to 300nm and has been previously published [22]. The solar simulator is class B in that it provides uniformity illumination across the 210mm × 210mm sample plane to within ±5%. For this work, the measured variation in power density over the fully-illuminated 100 mm × 100mm areas used for LSC measurement is actually within the class A specification of ±2%. A holder is used to clamp the LSC, ensuring minimal contact with the LSC sheet and thus preventing light from escaping at the point of contact. An optical fibre (∅600µm, Ocean Optics, USA) with a cosine corrector (CC-3-UV, Ocean Optics, USA) is held firmly against the edge of the LSC sheet, and is then connected to a spectrometer (HR2000CG-UV-

NIR, Ocean Optics, USA) with a wavelength range of 200 – 1100nm and a resolution of 0.5nm. This creates an irradiance probe that can be used to measure the intensity of light normal to the probe surface, as is shown in Figure 3(a). The measurement setup (cosine corrector, fibre and spectrometer) is calibrated for wavelength using a mercury argon calibration source (Ocean Optics HG-1) and for irradiance against a calibrated tungsten halogen lamp (Ocean Optics LS-1-CA). The software (SpetraSuite, Ocean Optics) thus able to convert the measured intensity (photon counts per second) to into power density (W/m^2). Absorbance spectra of the LSC sheets are measured using a UV–visible–near-infrared (NIR) spectrophotometer (Perkin Elmer Lambda 950) with a data interval of 1nm.

There are several sources of error which limit the accuracy of the measurement such as offsets, drift or light source long term stability. The sample holder is used to increase the repeatability of the measurement and to minimize errors introduced by the operator. An error is introduced by the sample holder touching the sample but this error is negligible since only 1% of the total bottom surface of the LSC sample is in touch with the holder. The main source of error is the solar simulator spectrum which has an irradiance uniformity of ±2% over the sample area and a temporal stability of 1%.

Table 1: Overview of PMMA LSC samples that were fabricated for this research, and then also used as an input for the ray-tracing simulations. For each dye type and concentration (given in both ppm and mol/L), a square (100mm × 100mm × 3mm) and circle (∅100mm, 3mm thick) were fabricated. Also given are the measured absorbance (OD) at the peak absorption wavelength of each dye (λ_{abs_peak}).

Dye (λ_{abs_peak})	Desired OD of LSC	Dye concentration required to achieved OD		Measured absorbance
		(ppm)	(mol/L)	
Violet 574 - 395) nm	0.05	4.5	1.41×10^{-5}	0.09
	1	91	2.82×10^{-4}	1.36
	2	181	5.63×10^{-4}	2.40
	3	272	8.45×10^{-4}	2.70
	4	362	1.13×10^{-3}	3.02
	8	725	2.25×10^{-3}	3.01
	16	1449	4.50×10^{-3}	3.01
Yellow 083 (474 - 489) nm	0.05	2.4	5.60×10^{-6}	0.05
	1	49	1.12×10^{-4}	0.83
	2	98	2.24×10^{-4}	1.80
	3	147	3.36×10^{-4}	2.90
	4	196	4.48×10^{-4}	2.90
	8	393	8.96×10^{-4}	3.10
	16	783	1.79×10^{-3}	3.10
Yellow 170 (498 - 514) nm	0.05	2.5	5.57×10^{-6}	0.08
	1	49	1.11×10^{-4}	1.40
	2	98	2.23×10^{-4}	2.80
	3	147	3.34×10^{-4}	2.80
	4	197	4.46×10^{-4}	3.09
	8	393	8.91×10^{-4}	3.10
	16	786	1.78×10^{-3}	3.10
Orange 240 (560 - 570) nm	0.05	1.8	2.96×10^{-6}	0.05
	1	13	5.92×10^{-5}	1.20
	2	37	1.18×10^{-4}	2.20
	3	110	4.77×10^{-4}	3.70
	4	146	2.37×10^{-4}	3.10
	8	293	4.74×10^{-4}	3.16
	16	586	9.47×10^{-4}	3.18
Red 305 (571- 585) nm	0.05	4.9	5.24×10^{-6}	0.19
	1	98	1.05×10^{-4}	1.19
	2	197	2.10×10^{-4}	2.50
	3	295	3.15×10^{-4}	3.19
	4	393	4.19×10^{-4}	3.31
	8	787	8.39×10^{-4}	3.33
	16	1574	1.68×10^{-3}	3.40

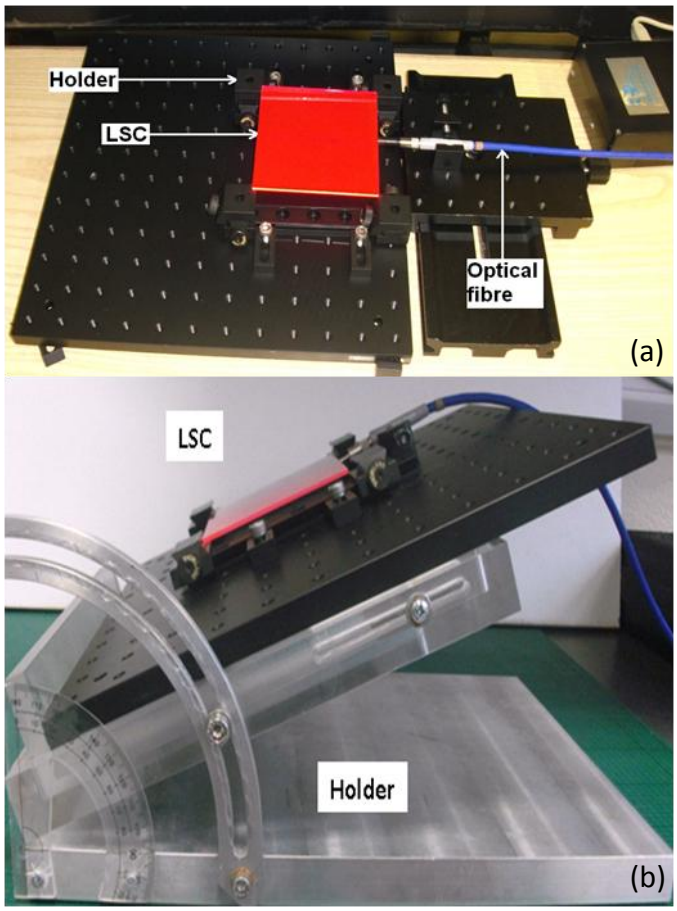

Figure 3: (a) Set up for the experimental measurement of LSC edge emission via cosine corrector and optical fibre; (b) the sample holder used for the tilt angle variation test.

4. Results and discussions

a. Dye concentrations and Colours

An example of the absorbance spectra for the 3mm-thick square LSC doped with all concentrations of the Red 305 dye is shown in Figure 4(a). The absorbance is seen to increase steadily with dye concentration, however at about 393ppm it starts to saturate at the dye absorption peak. This is likely to be due to the sensitivity of the spectrophotometer not being sufficient enough to resolve absorbances greater than about 3.5 – 4 (corresponding to >99.7% light absorption). The measured absorbance at the peak absorption wavelength of each dye is summarised in Table 1. At higher concentrations, the absorption shoulder at 535nm and other weaker peak at 440nm continue to increase in intensity, only exhibiting signs of saturation at the highest dye concentration (1574ppm). The irradiance spectra shown in Figure 4(b), where at the lowest dye concentration the emission peak is at 615nm. This is seen to shift significantly at higher dye concentrations: from 647nm at 98ppm, to 662nm at 1574ppm. The highest irradiance is measured for the 787ppm sample with a peak at 660nm, while a decrease in emission intensity is observed for the 1574ppm sample to due re-absorption losses. Absorbance and irradiance graphs for the other dyes of Violet 570, Yellow 083, Yellow 170 and Orange 240 are displayed in Figures S1 – S4 of the supplementary material.

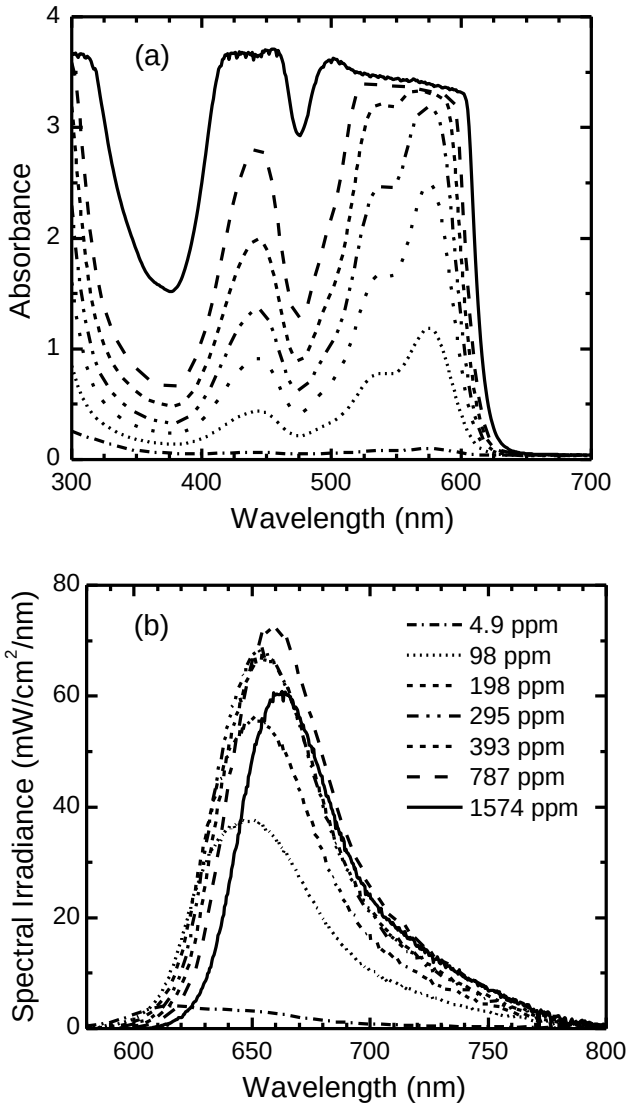

Figure 4(a) Absorption and (b) irradiance spectra for square LSC sheets containing different concentrations of Red 305 dye.

In Figure 5, the subset of colours of the 35 different dye concentrations is presented using the CIE (International Commission on Illumination) 1931 chart. The x, y and z coordinates are calculated using the CIE XYZ colour system values [23]. This graph provides the entire gamut of the five colours and their concentrations within the CIE colour space. It can be seen that an almost continuous range of colours can be achieved from green to red, however the range within the blue region is limited.

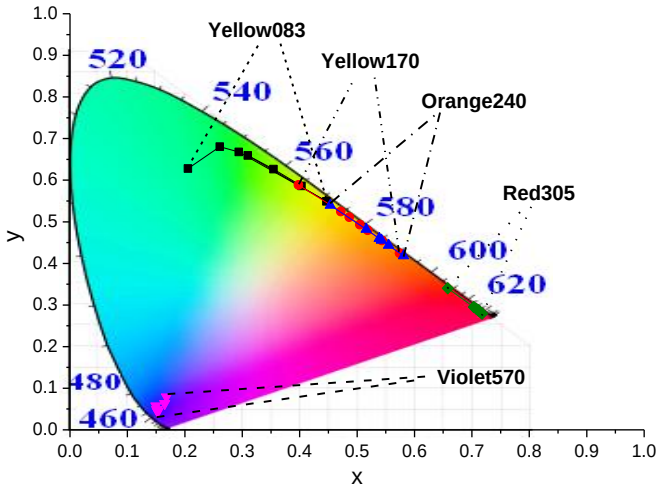

Figure 5: Gamut of the location of the colours achieved with the 35 Lumogen dye concentrations on the CIE 1931 xy chromaticity diagram.

The edge emission was measured for all the LSC samples listed in Table 1, and subsequently compared to the power density determined from the 3D ray-tracing simulation. Figure 6 shows the results of a comparison between simulation and experimental measurement for the whole range of colours and dyes concentrations, as well as for the two different LSC geometries.

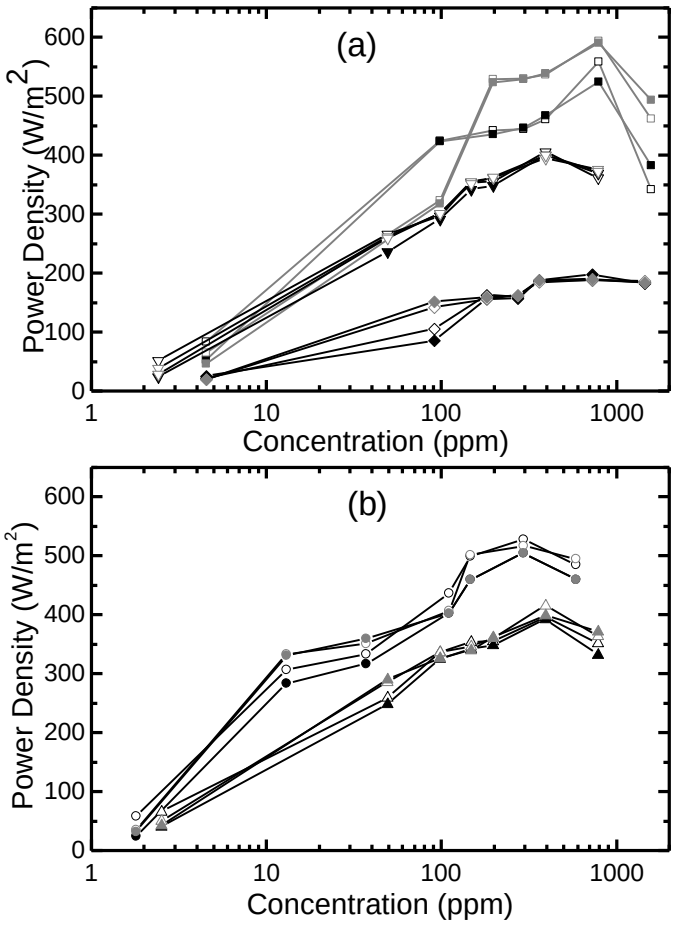

Figure 6: A comparison between simulations (hollow symbols) and experimental measurements (solid symbols) for the LSC samples (Black for square and Grey for circle) containing the following

dyes: (a) Violet 570 (◆, ◇); Yellow083 (▼,▽) and Red 305 (■,□). (b) Yellow 170 (▲,△) and Orange240 (●,○).

The trends found in these graphs are similar for all dyes. Firstly, the overall measured power density increases as the dye absorption extends towards longer wavelengths. Hence, the Red 305 doped LSCs exhibit the greatest overall power densities at higher dye concentrations and Orange240 at lower concentrations. Secondly, the measured edge emission increases with increasing dye concentration, up to the second highest value (corresponding to OD 8). At the highest dye concentration (OD 16), the edge emission intensity invariably decreases. This is confirmed by both by experimental measurements and simulation results and is attributed to the very high dye concentration used, giving rise to increased re-absorption losses [21]. Notably, no evidence of the formation of non-luminescent dye aggregates that parasitically absorb the luminescence [21] were observed as these would be observed in the experimental results but not in the simulations. Thirdly, the emitted optical power densities for the circular LSCs are typically slightly higher than for the equivalent square LSC. This is simply due to a circular LSC having the shortest average pathlength for emitted photons to reach the edge [24]. Note however, that there is variation between the measured power density for the square and circular LSCs and this is thought to arise from slight inconsistencies in the edge polishing between the two shapes. The circle LSC's seems to be perfectly cut whereas some of the square LSC's are not.

The ray-tracing simulations do not take into account several real-world losses, such as scattering arising from i) imperfections in the top and bottom LSC surfaces, ii) inclusions within the bulk of the sheet, iii) imperfect edge polishing, iv) inadequate *n* and *k* values for the PMMA as well as v) the spectral differences of the solar simulator.

In general, the impact of the host material refractive index to the results is negligible. The model shows that changes in power density using values from different other PMMA manufacturers (such as Lucite or Roehm/Evonik) are around ±0.1%. However, changes in extinction coefficient have a large impact at lower dye concentrations, with model showing an underestimation of -15% between simulation and experimental results. Also, the difference between the use of solar simulation spectrum and the standard AM1.5G plays a major role to define the performance of LSC's. The optical efficiency using the solar simulator spectrum is about 3% (relative) higher than when using the AM1.5G spectrum. This is due to the difference between the two curves on the peak absorption wavelength for each dye. However, the solar simulator spectrum is used by the software to compare between the simulation and the experiment. The software does not taken into consideration other limitations such as the contact between LSC samples and the holder, the reflection from the holder, the non-uniformity of the source and imperfect surfaces which leads to internal total reflection losses.

Despite these limitations, the maximum relative differences between the measured versus simulated power density was determined to be within ±13%, as shown in Figure 7. In addition, apart from low concentrations (OD 0.05), two-thirds of the comparative results are found to lie within ±5%. This difference between predicted and observed measurements shows a better agreement within the same range of dye concentration compared with those achieved by other groups such as [10]. Also, the modelling process here applies a 3D textures generator which can combine any shapes, surfaces,

materials, and orientations. This leads to a much reduced computation time, compared to other modelling of individual luminescent dyes, such as in the work of [25].

The main addition to former ray-tracing modelling methods is the use of sample measurement of the absorption and emission at low concentration (20ppm) by the luminescent dyes. Then, the software takes these absorption and emission characteristics as references to generate different concentrations with simple addition operations. However, from Figure 7 it appears as if there is a trend for under-estimating LSC performance at low to medium dye concentrations and over-estimating performance at very high dye concentrations. This could be related to the probability of the host material absorption. At lower concentration than the reference (20ppm), more rays emitted by the dyes have a higher probability to be absorbed by the host material, and this is why underestimation has occurred. At higher concentration, the probability that the rays are absorbed by the host material is lower and this is why overestimation has occurred. Finally, it should be noted that in both the experimental setup and the simulation, an air gap exists between the edge of the LSC and the detector. This means that the power density determined above, underestimates the power density that would illuminate a solar cell on the edges. However, when fabricating a fully-working LSC, a textured high-efficiency silicon solar cell would be optically-coupled to the edge of the LSC and the reflectance losses would be extremely small, even at angles of very high incidence such as 80° [26].

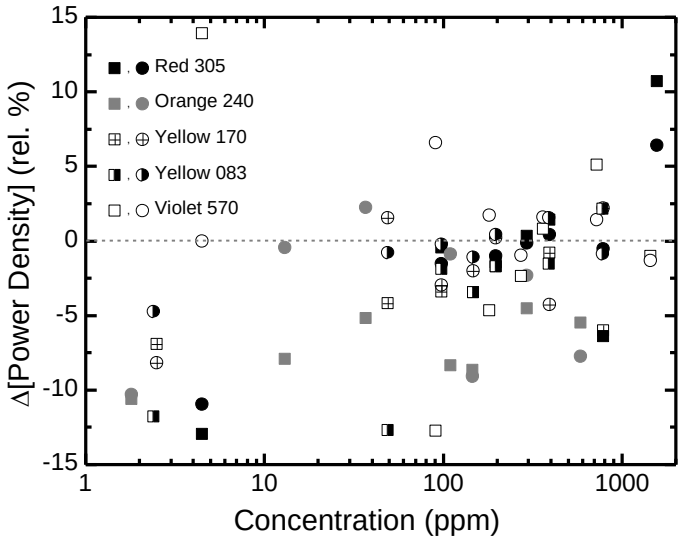

Figure 7: Relative difference in power density determined by ray-tracing simulations and measured experimental results.

b. Tilt angle variation

Many techniques are available to calculate the distribution of radiation within buildings. However, innovative architectural developments need more comprehensive information in the use of daylight by integration realistic prediction methods. Therefore, the appropriate calculations and the optimum solar concentrator design can provide a reduction in energy costs. In the previous results, the source illumination is normally incident upon the top surface of the LSC samples. However, for BIPV applications such as façades and windows, it is important to understand the variation in power density and optical efficiency with increasing tilt angles. As shown in Figure 3(b), the position of

the square LSC (Red 305, 787ppm) can be varied from 0° to 70° from the horizontal. The optical fibre is placed on the raised edge of the LSC in order to ensure that no stray light is collected directly from the solar simulator.

The incident power on the top of the LSC as it is rotated is related to the cosine of the incident angle. This power is calculated by the software using a detector which is placed on the top surface of the LSC. The optical efficiency is defined as the ratio of the incident power at the top surface (100 mm x 100 mm) to the collected power at the LSC edge (100mm x 3mm). Figure 8 illustrates that the prediction of the simulation is in good agreement with the experimental results: the difference between the two curves remains less than 7%.

As the tilt angle increases, the power density decreases as shown in Figure 8(a). This is due to less light incident on the collector front surface and reflectance losses when the LSC is tilted. On the other hand, the optical efficiency increases, as shown in Figure 8(b). This is due to the LSC emission output decreases more slowly than the measured incident power density at higher tilt angles. Also, by tilting the LSC, this leads to a longer effective path of the incident light inside the collector thus increasing absorption without increasing reabsorption. In addition to this, the model shows that the bottom surface of the square LSC becomes more of a reflecting surface than a transmitting surface. Rays are reflected from the bottom and the side surfaces of the LSC sheet. Experimental results show that the black optical breadboard holder reflects 5.73% at 0°, and when it is tilted more than 0°, the reflection from the holder is around 7%. This means that rays have more probability of interacting with the dyes at decreased angles of incidence.

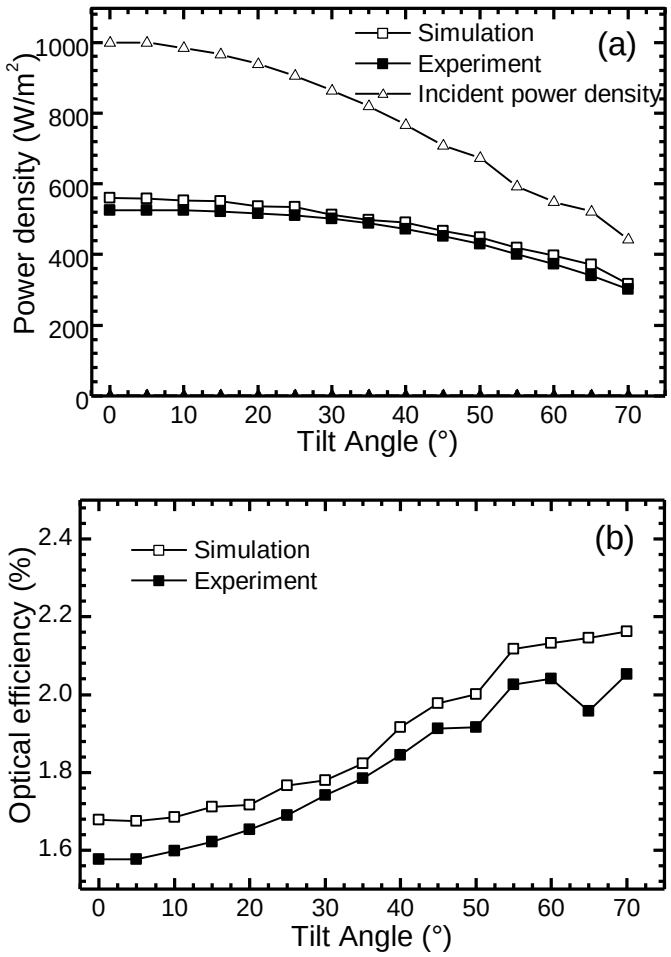

Figure 8: Comparison between simulated and experimental results for variation of the tilt angle of the square LSC (Red 305, 787ppm): (a) power density and (b) optical efficiency.

c. Stained-glass window modelling

In this section, the stained glass window shown in Figure 2 is modelled using the actual window dimensions 47cm x 58cm x 0.3cm. The five colours are distributed to create a similar pattern as the window design as shown in Figure 9, replacing the green colour by Yellow 083 and the clear glass by Violet570. The dye concentration corresponds to the optimum for each colour as shown in Table 2. The AM1.5G illumination source (1000 W/m^2) used in this simulation is tilted from -90° to 90° (a simplified solar day). The incident power is calculated by the software using a detector placed on the top surface of the window. The collected power density is calculated by placing the software detectors along the four edges of the window. The optical efficiency is defined as the ratio of the incident power at the top surface (2726 cm^2) to the collected power at the four LSC window edges (63cm^2).

Table 2: Concentrations and surface areas of the five colours used for the modelling

Dye	**Concentration**	**Surface area**
Violet570	725ppm	35% of the total surface
Yellow083	393ppm	25% of the total surface
Yellow170	393ppm	15% of the total surface
Orange240	293ppm	10% of the total surface
Red305	787ppm	15% of the total surface

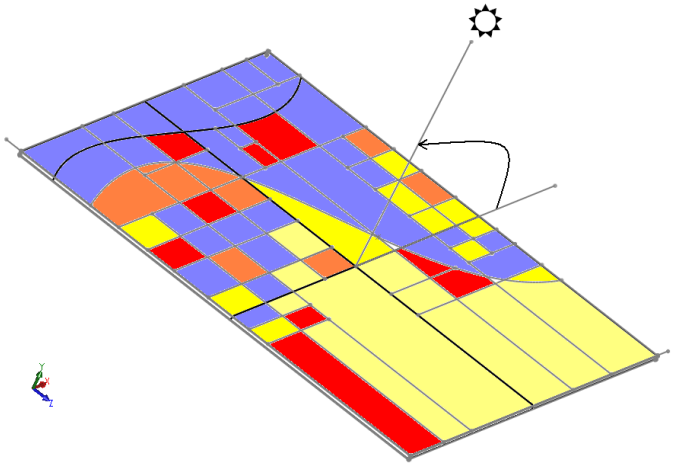

Figure 9: The stained glass window design modelled using five Lumogen dye colours.

Figure 10 illustrates the optical efficiency and the power density reaches the four edges of the window. As the source angle increased from 0° to 90°, the power density is decreased and the optical efficiency is increased; and vice versa when the source is directed from -90° to 0°. These results correspond well with the previous experiment when the tilt angle is changing from 0° to 70°. The window provides the highest power density when it is normally incident to the sun. However, the window is still capable of collecting light when the solar angle of incidence is tilted with relatively higher efficiency up to 6%. So, this LSC window design can generate electricity at a wide range of incident light angles and the actual peak (optical) power produced by this window is 5.0 Watt.

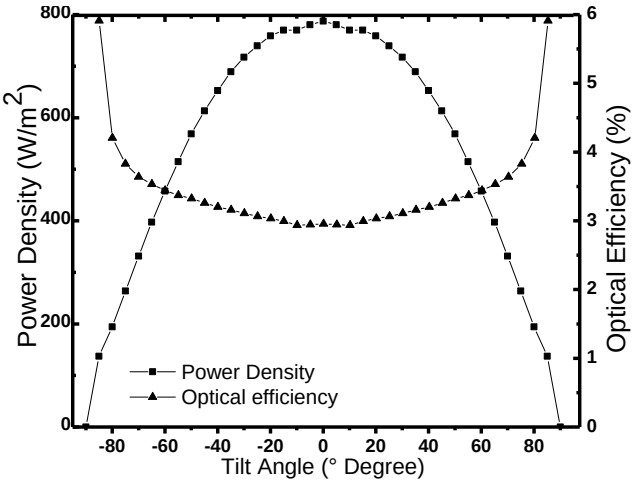

Figure 10: Power density and optical efficiency of a square stained glass window (47cm x 58cm x 0.5cm) for varying the tilt angle (-90° to 90°).

5. Summary

The focus in this work is directed towards the use of 3D ray-tracing software to gain deeper knowledge about the use of colours to create an aesthetic effect. This paper presents a comparison between a 3D ray-trace modelling using Optisworks and experimental test measurement of 70 different LSC sheets. Two different LSC geometries (square, circle) are fabricated with five different dyes at seven different dye concentrations each. The colour distribution of the samples used in this paper is presented in the CIE 1931 colour space. Overall, there is excellent agreement between the simulations and experimental results, with the maximum relative difference between the measured versus simulated edge emission power density determined to be around ±5% within a certain concentration range and a maximum difference of ±13%. Also, the power density and the optical efficiency when the LSC is tilted from 0° (normally incident light) up to 70° are investigated. The results show that the power density collected at the LSC edge had the highest value when the source is perpendicular to the sample. However, the optical efficiency increases at higher tilt angle. Again, the simulations are in agreement to within 7% of the measured experimental values. Finally, based on the different dye colours investigated, a model of a stained glass window is designed by the software and modelled throughout a solar day. Overall, the good agreement between the experimental data and the calculated values is obtained, which confirms that our ray-tracing models could now be extended to more ambitious shapes and the sizes in order to optimise the design of a LSC for application in the built environment.

6. Acknowledgement

This work is funded by the Leverhulme Trust. BASF (Germany) and Chilin (Taiwan) are thanked for providing the Lumogen dyes and fabricating the LSCs used in this study, respectively.

7. References

[1] A. Luque, G. Sala, I. Luque-Heredia , Photovoltaic concentration at the onset of its commercial deployment, Prog. Photovolt. 14 (2006) 413–428.

[2] W.H. Weber, J. Lambe, Luminescent greenhouse collector for solar radiation, J. Appl. Opt. 15, no. 10 (1976) 2299–2300.

[3] A. Goetzberger, W. Greubel, Solar energy conversion with fluorescent concentrators, J. Appl. Phys. 14, (1977) 123–129.

[4] M.G. Debije, P.P.C. Verbunt, Thirty Years of Luminescent Solar Concentrator Research: Solar Energy for the Built Environment, Adv. Energy Mater. 2 (2012) 12–35.

[5] W.G.J.H.M. Van Sark, et al., Luminescent Solar Concentrators: A Review of Recent Results, J. Optics Express. 16, Issue 26, (2008) 21773-21792.

[6] B.C. Rowan, L.R. Wilson, B.S. Richards, Advanced Material Concepts for Luminescent Solar Concentrators. IEEE Journal of selected topics in quantum electronics, 14, No. 5 (2008) 1312-1322.

[7] J.C. Goldschmidt, et al.. Advanced fluorescent concentrator system design, Proceedings of the 22nd European Photovoltaic Solar Energy: Conference, (2007) 608–612.

[8] M. Pravettoni, et al., Classical behaviour of output light emitted by the edge of a luminescent solar concentrator, 33rd IEEE Photovoltaic Specialists Conference (2008) 1–5.

[9] A.J. Chatten, et al., Quantum Dot Solar Concentrators, J. Semiconductors, 38 (2004) 609-617.

[10] K. Heidler, Efficiency and Concentration Ratio Measurements of Fluorescent Solar Concentrators Using a Xenon Measurement System, J. Appl. Opt. 20, No. 5 (1981) 773-777.

[11] M. Carrascosa, S.Unamuno, F. Agullo-Lopez, Monte Carlo simulation of the performance of PMMA luminescent solar collectors, J. Appl. Opt. 22, (1983) 3236-3241.

[12] A. Burgers, L. Slooff, A. Buchtemann, and J. van Roosmalen, Performance of Single Layer Luminescent Concentrators with Multiple Dyes, In Conference Record of the 2006 IEEE 4th World Conference on Photovoltaic Energy Conversion (2006) 198–201.

[13] M. Kennedy et al., Ray Trace Modelling of Multiple Dyes in a Luminescent Solar Concentrator, Proceedings of the 23rd European Photovoltaic Solar Energy Conference (2008).

[14] D. Şahin, B. Ilan, D.F. Kelley, Monte-Carlo simulations of light propagation in luminescent solar concentrators based on semiconductor nanoparticles, J. Applied Physics 110 (2011) 033108-1 - 033108-8.

[15] T.J.J. Meyer, J. Hlavaty, L. Smith ,E.R. Freniere, T. Markvart , Ray racing techniques applied to the modelling of fluorescent solar collectors, Proc. SPIE, Vol. 7211, (2009) 72110N-72110N-11.

[16] K.R. McIntosh, N. Yamada, B.S. Richards, Theoretical Comparison of Cylindrical and Planar Luminescent Solar Concentrators, J. Applied Physics B. 88(2), (2007) 285-290.

[17] L.R. Wilson, B.S. Richards, Measurement method for photo luminescent quantum yields of fluorescent organic dyes inpolymethylmethacrylate for luminescent solar concentrators, J. Applied Optics. 48, (2009) 212–220.

[18] J. N. Demas and G. A. Crosby, The measurement of photolumineseence quantum yields. A review, The J. of Physical Chemistry, 75 no. 8 (1971) 991–1024.

[19] Lumogen F series organic dye data sheets, http://www2.basf.us/additives/pdfs/p3201e.pdf. Last accessed 19/03/2013.

[20] G. Seybold, G. Wagenblast, New perylene and violanthrone dyestuffs for fluorescent collectors, J. Dyes and Pigments. 11, Issue 4, (1989) 303–317.

[21] L.R. Wilson, et al., Characterization and reduction of reabsorption losses in luminescent solar concentrators, J. Applied Optics, 49(9) (2010) 1651-1661.

[22] D. Ross, E. Klampaftis, J. Fritsche, M. Bauer b, B. Richards, Increased short-circuit current density of production line CdTe mini-module through luminescent down shifting, J. Solar Energy Materials & Solar Cells 103(2012)11–16.

[23] http://www.cie.co.at/index.php/LEFTMENUE/About+us/index.php. Last accessed 13/08/2013.

[24] E. Loh, D.J. Scalapino, Luminescent solar concentrators: effects of shape on efficiency, J. Applied Optics, 25(12), (1986) 1901-1907.

[25] M. Bendig, J. Hanika, H. Dammertz, J. C. Goldschmidt, M. Peters and M. Weber, in IEEE Symposium on Interactive Ray Tracing, IEEE, Los Angeles, CA, USA (2008) 93–98.

[26] A. Parretta et al., Optics Communications, 172 (1999) 139-151.

[27] http://www.carolarnold.co.uk/showdoc.asp@docid=87211245&catid=7.htm . Last accessed 16/08/2013.

Luminescent Solar Concentrators: from Experimental Validation of 3D Ray-Tracing Simulations to Coloured Stained-Glass Windows for BIPV

A. Kerrouche[1], D.A. Hardy[1], D. Ross[1], B. S. Richards[1,2]

[1] School of Engineering and Physical Sciences, Heriot-Watt University, Edinburgh, EH14 4AS, United Kingdom

[2] Department of Materials Science & Engineering Nelson Mandela African Institute of Science and Technology, Tengeru, Arusha, Tanzania

Supplementary Information

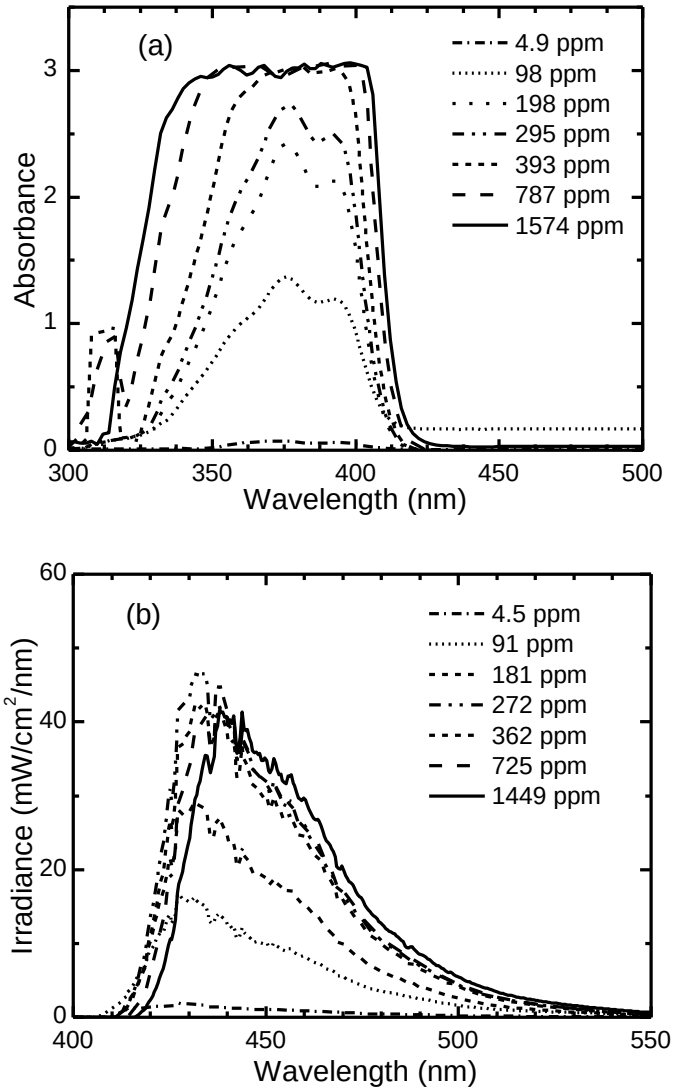

Figure S1 (a) Absorption and (b) irradiance spectra for square LSC sheets containing different concentrations of Violet 570 dye.

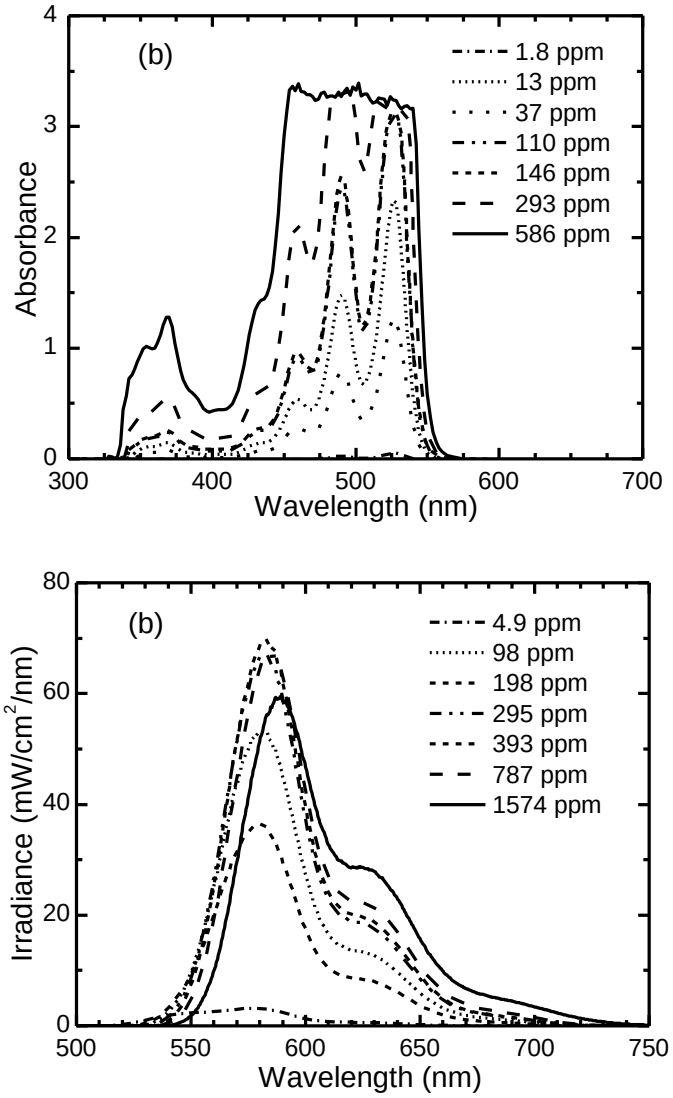

Figure S2 (a) Absorption and (b) irradiance spectra for square LSC sheets containing different concentrations of Orange240 dye.

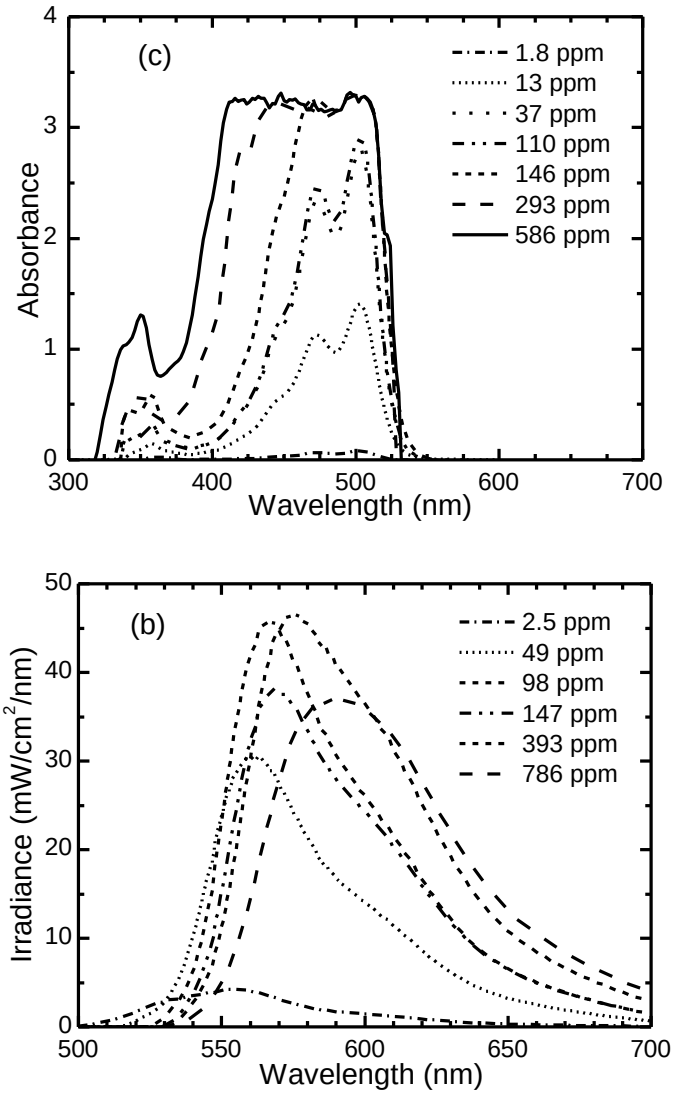

Figure S3 (a) Absorption and (b) irradiance spectra for square LSC sheets containing different concentrations of Yellow170 dye.

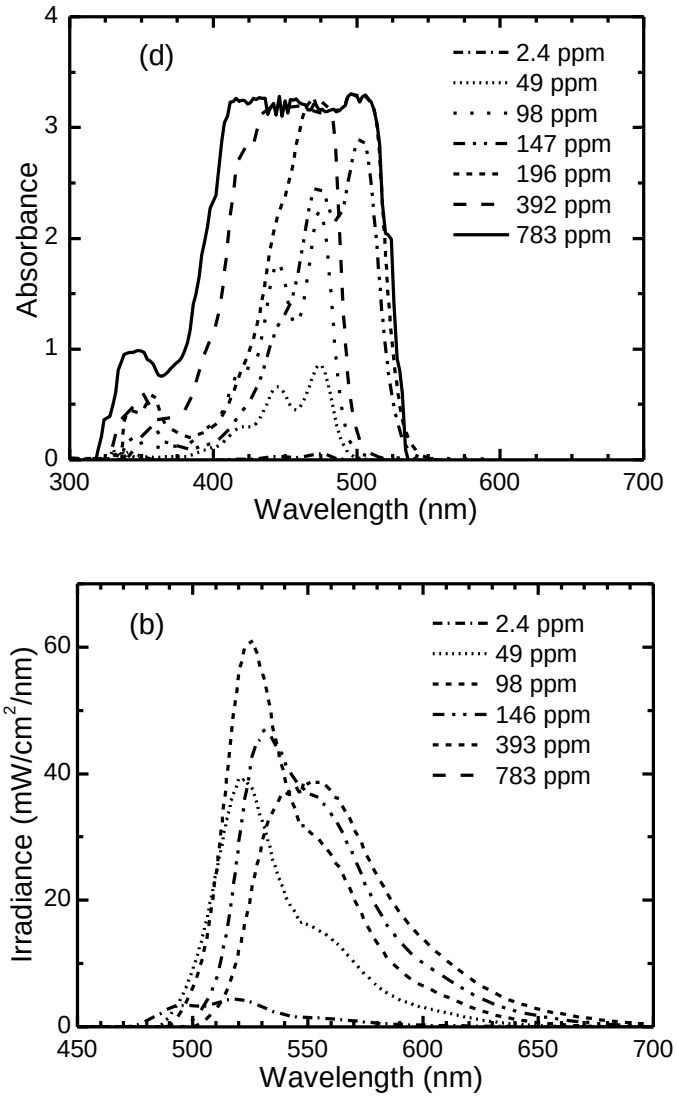

Figure S4 (a) Absorption and (b) irradiance spectra for square LSC sheets containing different concentrations of Yellow 083 dye.